

Molecular insights into the binding of coenzyme F₄₂₀ to the conserved protein Rv1155 from *Mycobacterium tuberculosis*

Ellene H. Mashalidis,^{1,2} Apostolos G. Gittis,³ Aurelie Tomczak,⁴ Chris Abell,² Clifton E. Barry III, and David N. Garboczi^{3*}

¹Tuberculosis Research Section, National Institute of Allergy and Infectious Diseases, Bethesda, Maryland 20892

²Department of Chemistry, University of Cambridge, Cambridge CB2 1EW, United Kingdom

³Structural Biology Section, Research Technologies Branch, National Institute of Allergy and Infectious Diseases, Rockville, Maryland 20852

⁴Molecular Signaling Section, Laboratory of Molecular Immunology, National Institute of Allergy and Infectious Diseases, Bethesda, Maryland 20892

Received 17 October 2014; Revised 17 January 2015; Accepted 20 January 2015

DOI: 10.1002/pro.2645

Published online 31 January 2015 proteinscience.org

Abstract: Coenzyme F₄₂₀ is a deazaflavin hydride carrier with a lower reduction potential than most flavins. In *Mycobacterium tuberculosis* (*Mtb*), F₄₂₀ plays an important role in activating PA-824, an antituberculosis drug currently used in clinical trials. Although F₄₂₀ is important to *Mtb* redox metabolism, little is known about the enzymes that bind F₄₂₀ and the reactions that they catalyze. We have identified a novel F₄₂₀-binding protein, Rv1155, which is annotated in the *Mtb* genome sequence as a putative flavin mononucleotide (FMN)-binding protein. Using biophysical techniques, we have demonstrated that instead of binding FMN or other flavins, Rv1155 binds coenzyme F₄₂₀. The crystal structure of the complex of Rv1155 and F₄₂₀ reveals one F₄₂₀ molecule bound to each monomer of the Rv1155 dimer. Structural, biophysical, and bioinformatic analyses of the Rv1155–F₄₂₀ complex provide clues about its role in the bacterium.

Keywords: *Mycobacterium tuberculosis*; Rv1155; coenzyme F₄₂₀; conserved hypothetical protein

Abbreviations: CASTp, computed atlas of surface topography of proteins server; Dali, distance alignment matrix method; DDN, deazaflavin-dependent nitroreductases; DSF, differential scanning fluorimetry; F₄₂₀H₂, reduced F₄₂₀; FGD1, F₄₂₀-dependent glucose 6-phosphate dehydrogenase 1; His_{6x}, 6x-histidine; IPTG, isopropyl β-D-1-thiogalacto-pyranoside; ITC, isothermal titration calorimetry; LB, Luria broth; LLM, luciferase-like monooxygenases; MBP, maltose-binding protein; *Mtb*, *Mycobacterium tuberculosis*; PLP, pyridoxal 5'-phosphate; PNPOx, pyridoxine 5'-phosphate oxidases; r.m.s., root-mean-square; SEC, size exclusion chromatography; SPE, solid-phase extraction; STRING, search tool for retrieval of interacting genes/proteins; TB, tuberculosis; T_m, melting temperature

Additional Supporting Information may be found in the online version of this article.

Grant sponsor: Intramural Research Program of the NIH, NIAID.

*Correspondence to: David N. Garboczi, Twinbrook 2 Rm 110, 12441 Parklawn Drive, Rockville, MD 20852.

E-mail: dgarboczi@niaid.nih.gov

Introduction

The causative bacterium of tuberculosis (TB), *Mycobacterium tuberculosis* (*Mtb*), is among the most widely distributed human pathogens, with an estimated one-third of the world population having evidence of infection by the bacterium.¹ Drug-resistant strains of *Mtb* have emerged and pose a significant threat to the control of TB worldwide.² New antibiotics are urgently needed to stem the spread of drug-resistant *Mtb*.³ TB drug design strategies can benefit from taking advantage of biochemical processes present in *Mtb*, but absent in human cells. One rich area is the biochemistry of coenzyme F₄₂₀ or 7,8-didesmethyl-8-hydroxy 5-deazaflavin (Fig. 1), which is found in mycobacteria but not in humans. Coenzyme F₄₂₀ is involved in the activation of PA-824,⁶ a pro-drug that is currently used in human clinical trials for the treatment of tuberculosis.⁷

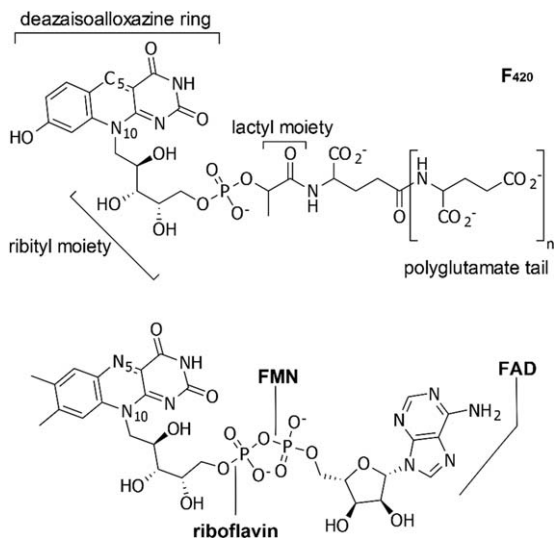


Figure 1. Coenzyme F₄₂₀ compared to the structures of three other flavins, riboflavin, FMN (flavin mononucleotide), and FAD (flavin adenine dinucleotide). Oxidized F₄₂₀ (upper) is shown. The predominant F₄₂₀ isoforms observed in mycobacteria have polyglutamate tails consisting of glutamates ($n = 5$ or 6) that are linked by γ -glutamyl bonds.^{4,5} In the lower panel are shown the oxidized structures of riboflavin, FMN, and FAD.

Coenzyme F₄₂₀ was first observed as a bright yellow and highly fluorescent pigment in mycobacteria in the early 1960s^{8,9} and was chemically identified after its purification from methanogenic Archaea.⁴ It is now known that F₄₂₀ is present in organisms from all three domains of life, archaea, bacteria, and eukaryotes, but it is relatively rare in nature overall. F₄₂₀ shares some structural similarities with more common flavins, such as riboflavin, flavin mononucleotide (FMN), and flavin adenine dinucleotide (FAD). However, the tricyclic ring system in F₄₂₀ differs from that of FMN and FAD in having a central carbon atom, C₅, at position 5 instead of a nitrogen atom as found in the other flavins (Fig. 1). For this reason, the F₄₂₀ ring system is referred to as a *deaza*alloxazine ring, and its ground-state reactivity typically involves hydride transfer to or from this site rather than the usual single electron chemistry of flavins.¹⁰ Other differences from more familiar flavins occur beyond the phosphate moiety, where F₄₂₀ has a lactyl group and polyglutamate tail using γ -glutamyl linkages (Fig. 1). Coenzyme F₄₂₀ has a lower reduction potential ($E^\circ \approx -360$ mV)¹¹ than most flavins and it has been suggested that this redox chemistry may help the bacterium survive in anaerobic conditions existing in human lesions.¹²

Little is known about the enzymes in *Mtb* that require coenzyme F₄₂₀ for catalysis. A comparative genomics study of *Mtb* suggests that there are at least 28 unique F₄₂₀-binding enzymes in *Mtb* that can be classified into three families: the deazaflavin-

dependent nitroreductases (DDN), the luciferase-like monooxygenases (LLM), and the pyridoxine 5'-phosphate oxidases (PNPOx).¹³ All three classes have homologs in other organisms that are known to bind either FMN or FAD. Examples from two of the classes have been studied. In the DDN family, Rv3547, also known as Ddn, is an F₄₂₀-dependent enzyme that catalyzes hydride transfer from the reduced coenzyme, F₄₂₀H₂, to the antituberculosis drug PA-824.¹⁴ In the LLM family, the F₄₂₀-dependent glucose 6-phosphate dehydrogenase 1 (FGD1, Rv0407) catalyzes the oxidation of glucose 6-phosphate and produces F₄₂₀H₂.^{15,16} At present, it appears that the only studies on F₄₂₀-dependent enzymes in *Mtb* are those on Ddn and FGD1, as no other F₄₂₀-dependent enzymes have been identified and characterized experimentally.

The PNPOx family in *Mtb* includes the gene products Rv1155, Rv2991, Rv2607, Rv0121c, Rv2061c, Rv1875, Rv2074, and Rv3369. All members of this class are annotated in the *Mtb* genome as conserved hypothetical FMN-binding enzymes. We previously demonstrated that Rv2607 functions as a canonical PNPOx, which catalyzes the oxidation of pyridoxine 5'-phosphate into the bioactive pyridoxal 5'-phosphate (PLP).¹⁷ The cofactor requirements of other *Mtb* proteins in the PNPOx-like class have not been experimentally confirmed; although crystal structures have been determined of Rv1155 without bound FMN¹⁸ and with bound FMN,¹⁹ it has remained unclear if Rv1155 binds FMN outside of a crystal environment.

Using biophysical techniques, we report here that Rv1155 binds coenzyme F₄₂₀ in solution, but does not bind FMN. In order to characterize the Rv1155-F₄₂₀ interaction, we determined the crystal structure of Rv1155 bound to F₄₂₀, which revealed how F₄₂₀ is bound and the importance of its polyglutamate tail in coenzyme recognition.

Results

Rv1155 does not co-purify with bound flavins

Two of the *Mtb* PNPOx family members, Rv1155 and Rv2607, were individually expressed in *Escherichia coli*. Both Rv1155 and Rv2607 were identified as homodimers by size exclusion chromatography (SEC). We have previously shown by mass spectrometry that Rv2607 as isolated from *E. coli* already contains bound FMN.¹⁷ The Rv2607-FMN complex has a UV-visible absorbance profile that is typical of an FMN-binding protein, which is characterized by two peaks in the ~350–500 nm region (Fig. 2). By contrast, Rv1155 lacks absorbance in this region, indicating that it does not co-purify with a flavin cofactor. As genes coding for enzymes involved in F₄₂₀ synthesis are absent in the *E. coli*

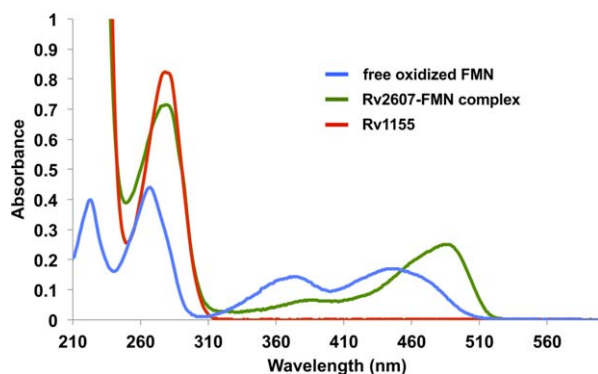


Figure 2. UV-visible absorbance spectra of Rv1155 and Rv2607, members of the *Mtb* PNPOx family, show that Rv1155 lacks the absorbance profile characteristic of an FMN-binding protein. The UV-visible spectrum of free, oxidized FMN (blue trace) has two peaks in ~ 350 – 500 nm region. The UV-visible spectrum of recombinant Rv2607 (green trace) has two peaks in the same part of the spectrum, which is consistent with Rv2607 being a known FMN-binding protein. Rv1155 (red trace) lacks absorbance in this region of the spectrum, indicating that it does not co-purify with a flavin when expressed recombinantly in *E. coli*. Free oxidized FMN, Rv2607-FMN, and Rv1155 are present at $30 \mu\text{M}$.

genome, neither Rv2607 nor Rv1155 would be expected to co-purify with F_{420} .

Rv1155 binds coenzyme F_{420}

Several redox cofactors were tested for binding to Rv1155 using differential scanning fluorimetry (DSF), including F_{420} , FMN, FAD, and nicotinamide adenine dinucleotide phosphate (NADPH) (Fig. 3). The intensity of the dye fluorescence versus temperature curve for Rv1155 has a stable baseline and sharp transition [Fig. 3(A)], making Rv1155 well suited for analysis using the DSF technique.²⁰ In the absence of cofactor, the melting temperature (T_m) of Rv1155 is 51.9°C [Fig. 3(A), blue trace]. In the presence of F_{420} ($50 \mu\text{M}$), the T_m of Rv1155

increased by 5.3° [Fig. 3(A), red trace]. This higher melting temperature indicates that F_{420} binding to Rv1155 increases the free energy of protein unfolding and thus renders Rv1155 resistant to denaturation at higher temperatures. The T_m of Rv1155 did not increase significantly in the presence of FMN, FAD, or NADPH [Fig. 3(B)], indicating that these cofactors do not similarly stabilize this protein.

The Rv1155- F_{420} binding interaction was further characterized by isothermal titration calorimetry (ITC) by titrating F_{420} into a $50 \mu\text{M}$ solution of Rv1155 (Fig. 4). Concentrations of Rv1155 $>50 \mu\text{M}$ resulted in significant aggregation of the protein as determined by dynamic light scattering. Fitting the ITC data to a one binding site model yielded a K_D of $170 \mu\text{M}$ for F_{420} binding to Rv1155. The measured binding affinity of F_{420} for Rv1155 is lower than that reported for the binding of F_{420} to other F_{420} -dependent proteins in *Mtb* (Ddn: $1 \mu\text{M}$,¹⁵ FGD1: $4.5 \mu\text{M}$ ²¹).

Trial enzymatic reactions with Rv1155 and F_{420}

Enzymatic test reactions were performed with Rv1155 in the presence of either reduced or oxidized coenzyme F_{420} . To detect a redox reaction mediated by Rv1155 and F_{420} , the oxidation state of F_{420} was monitored by absorbance at 420 nm. Oxidized F_{420} has a strong absorbance at 420 nm, but reduced F_{420} ($F_{420}\text{H}_2$) exhibits weak absorbance in this region. No change in the absorbance of oxidized or reduced F_{420} was observed in the presence of Rv1155 and pyridoxine 5'-phosphate, pyridoxamine 5'-phosphate, or PLP, indicating that Rv1155- F_{420} does not bind pyridoxine 5'-phosphate or its analogs as substrates. This is unlike other members in the PNPOx class that catalyze the oxidation of pyridoxine 5'-phosphate, including Rv2607 from *Mtb*.¹⁷ In the presence of reduced F_{420} , Rv1155 also does not metabolize the anti-TB drug PA-824, unlike the F_{420} -dependent nitroreductase Ddn, which does

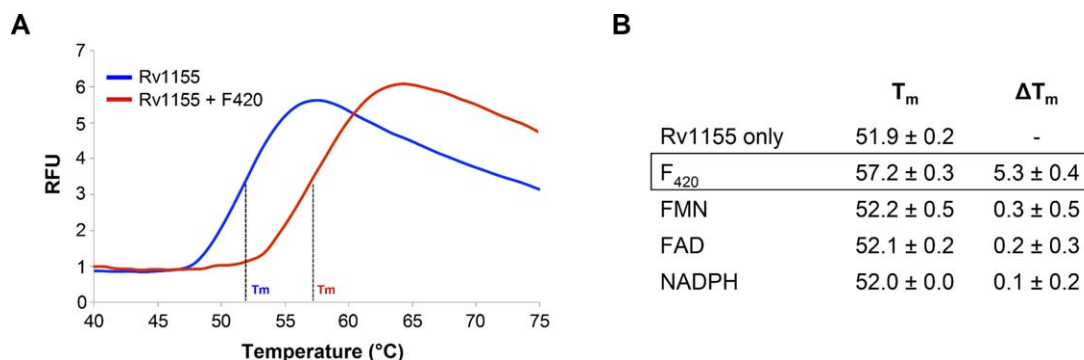


Figure 3. Rv1155 binds coenzyme F_{420} as assessed by differential scanning fluorimetry (DSF). (A) DSF melt curves in the presence of F_{420} (red trace) and in the absence of F_{420} (blue trace). Melt curves for FMN, FAD, and NADPH (not shown) were almost identical to the Rv1155 curve in the absence of F_{420} . (B) T_m values for Rv1155 in the presence of $50 \mu\text{M}$ F_{420} , FMN, FAD, and NADPH. The change in T_m (ΔT_m) was calculated relative to the Rv1155 only sample. Each measurement was made in triplicate. RFU, relative fluorescence units.

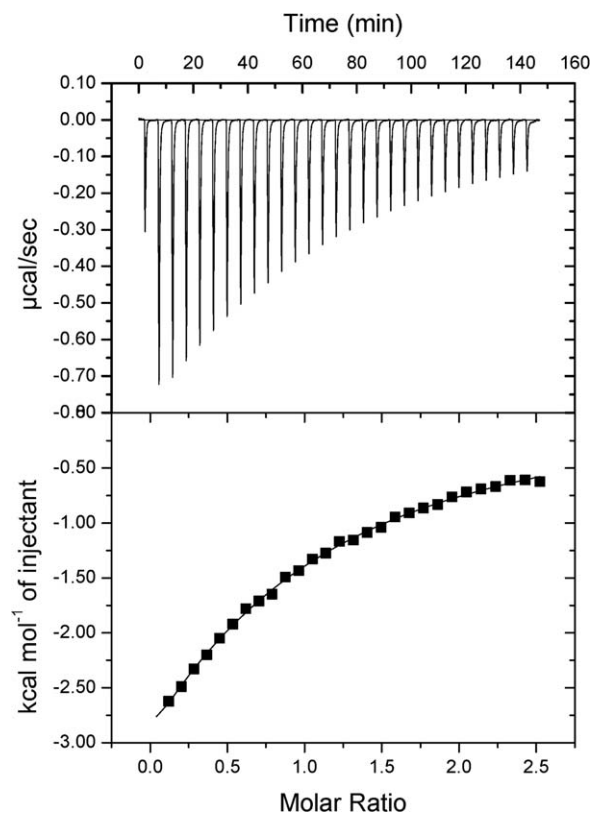


Figure 4. Isothermal titration calorimetry reveals the binding of F_{420} to Rv1155. The ligand, F_{420} (880 μM), was titrated into a solution of the protein, Rv1155 (50 μM as monomer). The top panel shows the ITC thermogram of the raw titration data that were measured for each injection of F_{420} . The data points in the bottom panel form the binding isotherm, in which each integrated peak area in units of kcal/mol is plotted against the ratio of the number of moles F_{420} that were injected to the number of moles of Rv115 present in the experiment. The solid line represents the best fit of the isotherm data to a one-binding-site model, which yielded a K_D value of 170 μM for the binding of F_{420} to Rv1155.

activate PA-824.¹⁴ MSMEG_5170, an ortholog of Rv1155 in *Mycobacterium smegmatis* with 79% sequence identity to Rv1155, carries out the reduction of α,β -unsaturated esters in aflatoxins in the presence of $F_{420}H_2$.²² However, we did not detect a change in the absorbance of reduced F_{420} with Rv1155 in the presence of the aflatoxin analogs, coumarin, 7-hydroxycoumarin, 7-hydroxy-4-methylcoumarin, or imperatorin.

Structure of Rv1155 with bound F_{420}

X-ray datasets were obtained from yellow crystals of the Rv1155- F_{420} complex, which diffracted X-rays to resolutions of 1.9–2.8 Å. An initial electron density map was obtained by molecular replacement. The Rv1155- F_{420} structure was refined at 2.3 Å resolution resulting in R -factors of 0.25 (R_{free}) and 0.19 (R_{work}) (Table I). One Rv1155 homodimer was present in the asymmetric unit of the Rv1155- F_{420}

crystals. There was continuous electron density in monomer A from Gln4A to Pro144A and in monomer B from Gln4B to Arg147B. At the interface between the monomers and near the surface of the dimer, there was difference electron density at two sites that enabled the unambiguous placement of two molecules of F_{420} [Fig. 5(A)]. For the molecule of F_{420} in binding site 1, we observed electron density for the deazaisalloxazine ring system, the ribityl moiety, the phosphate, the lactyl moiety, and one residue of the polyglutamate tail [Fig. 5(B)]. For the F_{420} molecule in binding site 2, we did not see electron density for the deazaisalloxazine ring system, but as in binding site 1, we observed difference electron density for the ribityl moiety, the phosphate, the lactyl moiety, and two glutamate residues out of the five or six residues in the polyglutamate tail of F_{420} [Fig. 5(C)]. Electron density was not observed in either site for the third glutamate and additional glutamates of the polyglutamate tail as they were likely disordered in the crystal.

Each F_{420} binding site is formed by residues from both Rv1155 monomers. The negative charge of the phosphate group and the first two residues of the polyglutamate tail of F_{420} are accommodated by a tunnel of positively charged and polar residues at the dimer interface. The portion of the polyglutamate tail visible in the structure makes hydrogen-bonding interactions with His27, Asn60, and His138 (Fig. 5). Several additional basic residues that could interact with additional glutamates in the polyglutamate tail are Arg30, Arg59, Arg63, and Arg66. The lactyl moiety of F_{420} forms a hydrogen bond with

Table I. Rv1155 X-Ray Data and Refinement Statistics

X-ray data	
X-ray source	APS 22-BM
Resolution limit (Å)	49–2.30 (2.36–2.30)
Space group	$P2_12_12_1$
Unit cell dimensions (Å)	53.6, 65.2, 77.1
Completeness (%)	99.8 (100)
Multiplicity	7.0
Wilson B -factor (Å ²)	45
R_{merge} (%)	3.7 (25.0)
$\langle I/\sigma(I) \rangle$	33.6 (8.5)
Refinement	
Resolution limits (Å)	33–2.30 (2.38–2.30)
No. of reflections in working set	12,470
No. of reflections in test set	634
R_{work} (%)	18.6 (22.1)
R_{free} (%)	25.2 (34.6)
Number of atoms	
Protein; H ₂ O; F_{420} and other	2206; 59; 138
Geometry r.m.s. deviations	
Bond lengths (Å)	0.008
Bond angles (°)	1.13
B -factors (Å ²)	
Monomer A	37.3
Monomer B	35.6
H ₂ O	37.8
F_{420} and other atoms	49.7

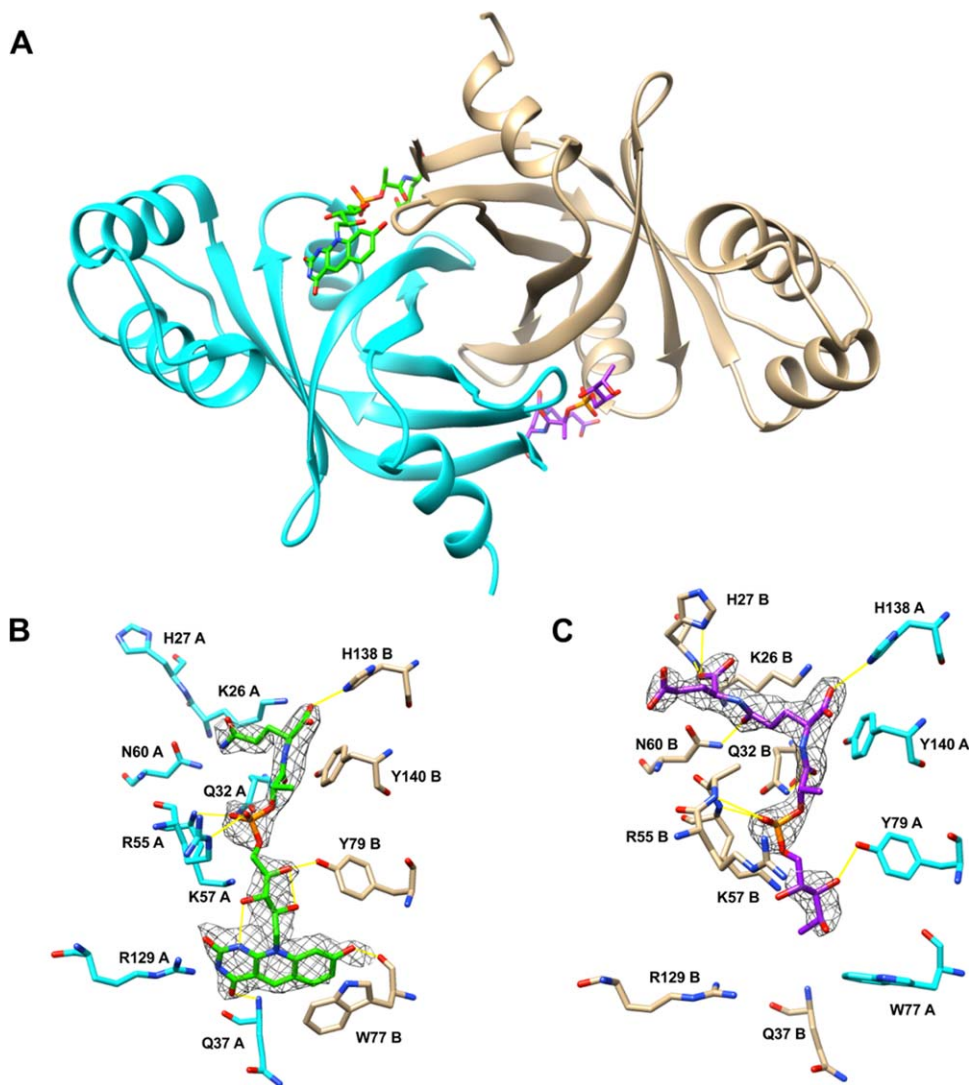


Figure 5. Crystal structure of Rv1155 bound to F_{420} at 2.3 Å resolution. (A) Structure of the Rv1155 homodimer with two F_{420} molecules (green, purple) bound at the interface between chain A (cyan) and chain B (tan). (B) Detailed view of binding site 1. (C) Detailed view of binding site 2. Electron density for the ring system of F_{420} is not visible in binding site 2 (see text). The $2F_o - F_c$ electron density for F_{420} is contoured at 1.0σ . Hydrogen bonds are represented as yellow lines.

Gln32 and the phosphate is held in place via hydrogen bonds to Arg55 and Lys57. The ribityl moiety interacts with Tyr79, hydrogen bonds with Lys57, and is stabilized by intra- F_{420} hydrogen bonds. The deazaalloxazine ring system forms hydrogen bonds with main chain atoms of Gln37 and Trp77. A stacking interaction occurs between the side chain of Trp77 and the benzene ring portion of the deazaflavin.

Even though the two coenzyme binding sites in Rv1155 are identical, there was little electron density for the deazaalloxazine ring of F_{420} in binding site 2. The positions of the Trp77 and Arg55 side chains in binding site 2 suggest that the F_{420} ring system in binding site 2 may be missing or disordered [compare Fig. 5(B) and 5(C)]. Rv1155- F_{420} crystals that were transferred to a cryoprotectant solution that was not supplemented with F_{420}

yielded structures with a bound F_{420} in binding site 2, but without a F_{420} in binding site 1. This observation indicates that the incomplete F_{420} in binding site 2 may have co-crystallized with the protein, while the F_{420} in binding site 1 may have soaked into its binding site.

The electron density for F_{420} in binding site 1 clearly demonstrates that the ring system assumes a conformation in which the two outer rings are bent relative to the central ring containing C_5 [Fig. 6(B)]. This “butterfly” conformation is commonly seen in protein-bound flavins.²⁴ The butterfly angle of the coenzyme F_{420} in the structure was determined to be 16.5° by measuring the angle between the mean planes of the central and benzene rings.²⁵

A substrate molecule that can be oxidized or reduced by F_{420} would likely bind near the deazaalloxazine ring system where hydride transfer is

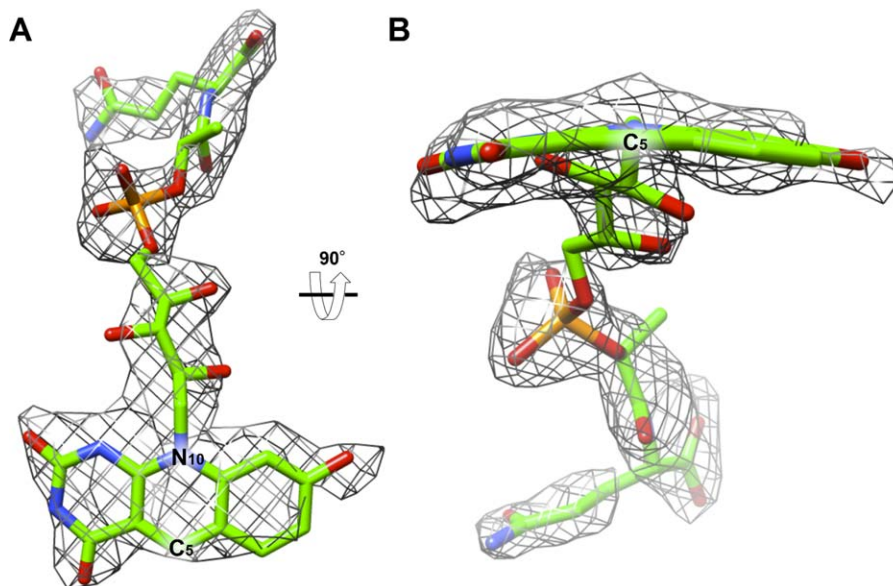


Figure 6. The $2F_o - F_c$ omit electron density of the F_{420} in the crystal structure of Rv1155 contoured at 1.0σ . (A) F_{420} modeled into the density found in the binding site 1 viewed from the interface of chains A and B. (B) F_{420} as viewed after 90° rotation around the horizontal axis relative to panel A. The density indicates that the ring assumes a butterfly conformation, meaning the ring system is not fully planar, but that the pyrimidine and benzene rings of the deazaalloxazine ring system are bent below the central ring, which contains C_5 and N_{10} . The butterfly angle is 16.5° , defined as the angle between the plane of the pyrimidine ring and the plane of the benzene ring. The angle was measured using Chimera.²³

known to occur in other proteins. Adjacent to the ring system in the structure there is a pocket lined with polar and hydrophobic residues where a substrate may bind (Fig. 7). The volume of the pocket is 130 \AA^3 as calculated using Computed Atlas of Surface Topography of proteins server (CASTp).²⁶ This pocket is formed by the small domain of the PNPOx-like fold, which is the known binding site of substrates PNP and PMP in the *E. coli*²⁷ and human²⁸ PNPOx enzymes.

Comparison of Rv1155- F_{420} complex with other structures

Rv1155- F_{420} was compared with all other structures deposited in the PDB using the distance alignment matrix method (Dali).²⁹ The PDB entries with the greatest global-fold similarity to Rv1155 are predominantly other PNPOx-like proteins of unknown function. The highest scoring hits were the two PNPOx-like proteins, Rv2991 and Rv2074 from *Mtb*, and one protein, MSMEG_3380, which is the *M. smegmatis* ortholog of Rv2074. The root-mean-square (r.m.s.) deviations on α -carbons of Rv2991 (PDBID: 1RFE), Rv2074 (PDBID: 2ASF³⁰), and MSMEG_3380 (PDBID: 3F7E²²) relative to Rv1155- F_{420} are 2.7, 2.5, and 2.6 \AA , respectively. The available X-ray crystal structures of Rv2991, Rv2074, and MSMEG_3380 have no bound cofactors or substrates. We superimposed the crystal structure of Rv1155- F_{420} with those of Rv2991, Rv2074, and MSMEG_3380 to compare the F_{420} binding site in Rv1155 to the analogous sites in the three other

mycobacterial PNPOx-like proteins. This analysis revealed that most of the residues in Rv1155 that interact with F_{420} [shown in Fig. 5(A,B)] are conserved in Rv2991, Rv2074, and MSMEG_3380. For example, Rv1155 residues Q32A, K57A, N60A, Y79B, R129A, and H138B are mostly conserved in Rv2991, Rv2074, and MSMEG_3380 (Table II). Based on the structural similarities that Rv2991 and Rv2074 share with Rv1155, we propose that

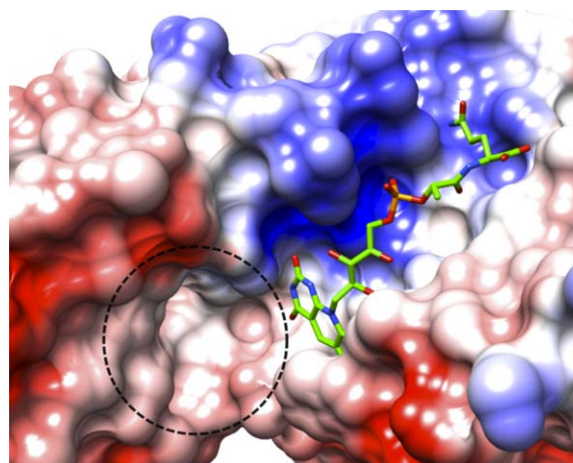


Figure 7. Putative active site in Rv1155- F_{420} . Surface representation of the Rv1155 colored by electrostatic potential (red, negative; blue, positive; white, neutral, which corresponds to areas occupied by polar or hydrophobic residues). The dashed line encircles a putative substrate-binding pocket near the F_{420} deazaalloxazine ring system, which has a volume of 130 \AA^3 .

Table II. Other PNPOx-Like Proteins in Mycobacteria Have Analogous Amino Acid Residues Positioned Similarly to Those of Rv1155 That Interact with the Coenzyme and May Also Bind F₄₂₀

Protein	F ₄₂₀ moieties					
	Lactyl	Ribityl, P	PolyGlu	Ribityl, P	Ring system	Lactyl, polyGlu
Rv1155	Q32A	K57A	N60A	Y79B	R129A	H138B
Rv2991 ^a	H38A	K61A	N64A	G86B	R132A	R141B
Rv2074 ^a	H36A	K61A	N60A	W81B	R117A	R126B
MSMEG_3380 ^a	Q30A	K53A	N56A	Y76B	A125B	R80B
Rv1875 ^b	Q30	K58	N61	W78	R133	R142
Rv0121c ^b	H28	R66	N69	W92	G129	R138

^a Analogous residues identified by structural superposition with Rv1155.

^b Analogous residues identified by sequence alignment with Rv1155.

Rv2991 and Rv2074 also bind coenzyme F₄₂₀. MSMEG_3380 is known to bind F₄₂₀H₂ and to use it to reduce alfatoxins.²² From its comparison with the Rv1155 structure, MSMEG_3380 likely binds F₄₂₀ at an analogous site. Crystal structures are not available for Rv1875 and Rv0121c, but sequence alignments indicate that they also bind F₄₂₀ (Table II).

Metabolic pathway analysis for Rv1155

Proteomic investigation has shown that Rv1155 is found in the membrane fraction of *Mtb* cell lysates.³¹ There is no signal sequence in Rv1155 to target it to the membrane, nor does it have any predicted transmembrane regions, amphipathic membrane anchors, or lipidation sites. In order to identify possible interaction partners that can localize Rv1155 to the membrane, a metabolic pathway analysis was performed on 1133 genomes using the Search Tool for Retrieval of Interacting Genes/Proteins (STRING) database³² (<http://string-db.org/>). One way to predict functional pathways is to compare gene co-occurrence across many genomes, that is, to identify genes that tend to be either present or absent together because they form a functional unit in the cell.³³ Of the 10 genes identified that co-occur with Rv1155, seven are also found in the membrane fraction of *Mtb* cells,³¹ including Ddn, a Ddn homolog Rv1558, and PNPOx-like proteins Rv2074 and Rv2061c (Supporting Information Table I). Like Rv1155, none of the co-occurring gene products contain predicted signal peptides or transmembrane regions.

Discussion

Rv1155 is a member of a class of proteins that are related to one another by a common domain type classified as “PNPOx-like” in the Pfam database³⁴ (Pfam ID: Pyridox_oxidase, PF01243). Selengut and Haft used computational techniques to identify potential F₄₂₀-dependent protein families in *Mtb* and to distinguish proteins that bind F₄₂₀ from those that recognize FMN.¹³ This approach pointed to Rv1155 as an F₄₂₀-binding protein along with other PNPOx-like proteins in *Mtb* (Rv2991, Rv0121c, Rv2061c, Rv1875, Rv2074, and Rv3369). Our data

provide experimental evidence for the use of F₄₂₀ by Rv1155. The remaining PNPOx-like proteins in *Mtb* may constitute a novel class of F₄₂₀-binding proteins.

The differential scanning fluorimetry assay demonstrated that the *T_m* of Rv1155 remains unchanged in the presence and absence of FMN, showing that FMN does not bind Rv1155. This result is consistent with the absorbance profile of pure recombinant Rv1155, which indicates that it does not co-purify with FMN when expressed in *E. coli*. These findings corroborate previous observations that Rv1155 does not behave as a canonical FMN-dependent enzyme,¹⁸ but they are conflicting with the reported structures of Rv1155–FMN (PDBID: 1Y30¹⁹) and Rv1155–PLP (PDBID: 2AQ6¹⁹). We suggest that the crystal structure of Rv1155 bound to FMN may be the result of weak FMN binding that is stabilized by the crystal lattice. Comparison of the Rv1155–FMN and Rv1155–F₄₂₀ structures shows that the phosphate moieties in FMN and F₄₂₀ bind at nearly the same site where they form hydrogen bonds with Arg55 and Lys57 (Supporting Information Fig. 1A). The ribityl moieties, which are identical in FMN and F₄₂₀, make the same hydrogen bond with Tyr79 in Rv1155. A structural superimposition of Rv1155–FMN and Rv1155–PLP showed that simultaneous binding of FMN and PLP is improbable because the molecules would occupy the same space in the binding site (Supporting Information Fig. 1B). In addition, FMN and PLP are found in only one of the two binding sites per Rv1155 homodimer.¹⁹

The present crystallographic data reveal that F₄₂₀ binds to Rv1155 at the homodimer interface on the surface of the protein. F₄₂₀ is accommodated by a cleft in the protein lined with basic residues that can form hydrogen bonds with the polyglutamate tail and the phosphate of F₄₂₀. The binding mode of F₄₂₀ in Rv1155 is similar to that of F₄₂₀ bound to Ddn (Supporting Information Fig. 2). Rv1155 and Ddn also share some global-fold similarities, including a beta-barrel core and a small, alpha helical domain, although the two proteins have only 12% sequence identity.

The butterfly bend angle of the flavin tricyclic ring system is related to its redox properties. The protein environment mediates the extent of ring puckering, which allows for fine-tuning of the reduction potential required to carry out its biological function.²⁵ The butterfly bend angle of F₄₂₀ in the structure is 16.5°. This value falls within the range of bend angles measured in other F₄₂₀-bound structures deposited in the Protein Databank: 13.9° (PDBID: 1JAY³⁵), 15.0° (PDBID: 3IQE³⁶), 20.4° (PDBID: 3B4Y¹⁵), 31.7° (PDBID: 1RHC³⁷), and 52.7° (PDBID: 1Z69³⁸). Flavins with larger bend angles tend to have lower reduction potentials.²⁵ Larger flavin butterfly bend angles are also associated with a less stable semiquinone (one electron) intermediate.²⁵ The semiquinone state is not observed in deazaflavins like F₄₂₀ because the radical anion at C₅ is too unstable.¹¹ F₄₂₀ is able to carry out low reduction potential reactions inaccessible by other flavins such as FMN and FAD.¹¹

The butterfly bend angle of the deazaalloxazine ring in the current structure provides some insight into the enzymatic properties of this enzyme-coenzyme system. Oxidized flavins tend to be more planar than the one- and two-electron reduced forms. The butterfly bend angle observed for F₄₂₀ bound to Rv1155 is similar to that (20.4°) of F₄₂₀-dependent glucose 6'-phosphate dehydrogenase from *Mtb* (PDBID: 3B4Y¹⁵), which catalyzes the reduction of F₄₂₀, and to that (15.0°) of F₄₂₀-dependent methylene-tetrahydromethanopterin dehydrogenase (PDBID: 3IQE³⁶) from *Methanopyrus kandleri*, which is capable of reversibly transferring a hydride using F₄₂₀ as the carrier. Rv1155 may exhibit similar redox properties to these F₄₂₀-dependent systems in which F₄₂₀ can be used as an oxidizing agent.

The precise enzymatic reaction catalyzed by Rv1155 remains unknown. Trial enzymatic reactions conducted with Rv1155 and reduced or oxidized F₄₂₀ have ruled out the possibility that Rv1155 can function as a PNPOx, a Ddn, or an enzyme capable of aflatoxin degradation. Adjacent to the F₄₂₀-binding pocket in Rv1155 is a hydrophobic cavity measuring 130 Å³ (Fig. 7). The pocket may be the site of substrate binding as it is located near the F₄₂₀ deazaalloxazine ring system responsible for redox chemistry. This putative substrate-binding space is similar in size to that of the F₄₂₀-dependent secondary alcohol dehydrogenase (128 Å³), which binds isopropanol (PDBID: 1RHC³⁷). Alternatively, this location may be where a partner protein may bind that would use the redox properties of the bound F₄₂₀.

Rv1155 is found in the membrane fraction of *Mtb* cell lysates,³¹ but analysis of its primary sequence reveals that it lacks features that target it to the membrane. In order to explore potential

functional roles for Rv1155, we used the STRING database to predict other gene products in *Mtb* that may participate in the same pathway as Rv1155. Some of the predicted pathway members may physically interact with Rv1155, particularly if they are located in the same subcellular region. The gene co-occurrence analysis on Rv1155 identified seven gene products that are experimentally confirmed membrane-associated proteins (Supporting Information Table I). It is possible that Rv1155 forms a complex with one or more membrane-associated proteins, which would tether it to the membrane and allow it to carry out its function in the bacterium.

The gene product Rv1155 was annotated in the *Mtb* genome as an FMN-binding protein belonging to the PNPOx family based on sequence comparison and previous structural analysis. We have provided experimental evidence showing that Rv1155 does not bind FMN nor does it exhibit canonical PNPOx activity, that is, oxidation of pyridoxine 5'-phosphate or pyridoxamine 5'-phosphate to produce PLP. Using biophysical and crystallographic methods, we have shown that Rv1155 instead binds to a redox deazaflavin coenzyme found in mycobacteria called F₄₂₀, and thus Rv1155 takes its place beside Ddn and FGD1 as one of a small number of experimentally validated F₄₂₀-binding proteins in *Mtb*.

Materials and Methods

Production and purification of F₄₂₀

The protocol for F₄₂₀ purification was developed by modifying existing procedures.^{39,40} *M. smegmatis* cells were transformed with genes *fbtA*, *fbtB*, and *fbtC*, which were obtained in a pYUBDuet vector from Prof. Edward N. Baker (University of Auckland, New Zealand). The genes *fbtA*, *fbtB*, and *fbtC* encode enzymes involved in the biosynthesis of F₄₂₀.⁴¹ The vector was electroporated into *M. smegmatis* strain mc²155 as previously described.⁴² *M. smegmatis* cells overexpressing the F₄₂₀ biosynthetic genes were grown in kilogram quantities in fermenters in Luria broth (LB) broth. When the culture reached an OD_{600nm} of 0.6, IPTG was added to a final concentration of 0.25 mM and further incubated for 2 days. For one round of purification, typically around 800 g of *M. smegmatis* transformed with *fbtABC* was thawed at 4°C and resuspended in a minimal volume of 25 mM potassium phosphate buffer pH 7.5, avoiding large clumps of cells (~1.6 L). The suspension was autoclaved (121°C) for 20 min, cooled at 4°C, and centrifuged at 40,000g for 50 min. The bright yellow supernatant was filtered with a 0.45-μm pore membrane filter (Millipore). The cell pellet was again resuspended in a minimal volume of 25 mM potassium phosphate buffer, pH

7.5 (~1 L) and the mixture was again autoclaved, centrifuged, and filtered as before.

The supernatants from both autoclave cycles were pooled and loaded onto a quaternary aminoethyl anion exchange column equilibrated with 25 mM potassium phosphate buffer pH 7.5 at a flow rate of 0.5 mL/min at 4°C. The column was then washed at a constant flow rate of 1 mL/min with 25 mM potassium phosphate buffer pH 7.5 containing increasing concentrations of NaCl. The column was first washed with 100 mM NaCl in potassium phosphate buffer (2 L). A precursor to F₄₂₀, F₀, was eluted with 250 mM NaCl in potassium phosphate buffer (2 L). The column was further washed with 400 mM NaCl (2 L) in potassium phosphate buffer. F₄₂₀ eluted from the column with 600 mM NaCl (2 L) potassium phosphate buffer. The eluate was monitored spectrophotometrically at $\lambda = 420$ nm and 300 or 500 mL fractions were collected. Each fraction was analyzed by LC-MS, which detected F₄₂₀ species with five glutamates, F₄₂₀-5 (*m/z*: 1161), and with six glutamates, F₄₂₀-6 (*m/z*: 1290). Under these conditions, *M. smegmatis* cells transformed with the vector containing *fbABC* have about five times higher F₄₂₀ production levels than do wild-type *M. smegmatis* cells.

The fractions containing F₄₂₀ were removed from the high salt buffer using solid-phase extraction (SPE) C18 cartridges according to the manufacturer's protocol (Waters SEP-Pak Long). Conductivity measurements indicated that the SPE cartridges removed 97% of salts in the sample. The desalted F₄₂₀ fractions were lyophilized and then dissolved in a minimal volume of water. The F₄₂₀ was further purified by reverse-phase HPLC on a Varian Prep Star instrument using a Phenomenex Luna C18 (250 × 21.20 mm², 10 μ m) column. Solution A was 0.1% formic acid in water and solution B was acetonitrile. The column was equilibrated with 95% solution A and 5% solution B for 2 min. The following linear elution gradients were used: 95–80% solution A and 5–20% solution B from 2 to 32 min, then 80–5% solution A and 20–95% solution B from 32 to 35 min, and 5% solution A and 95% solution B for 5 min. The fractions containing F₄₂₀ were pooled, lyophilized, and dissolved in a minimal volume of water. The concentration of F₄₂₀ was determined with the extinction coefficient⁴³ at 420 nm, which is 25.9 mM⁻¹ cm⁻¹. The purity of F₄₂₀ was assessed by LC-MS. Yield was determined to be 104 mg of F₄₂₀ per 800 g *M. smegmatis* cells overexpressing the F₄₂₀ biosynthetic genes.

Expression and purification of Rv1155

The Rv1155 bacterial expression plasmid was obtained as an amino terminal 6x-histidine (His_{6x})-maltose-binding protein (MBP) fusion construct with TEV protease cleavage site from Dr. Yves Bourne

(Architecture et Fonction des Macromolécules Biologiques, CNRS, Marseille, France).¹⁸ The Rv1155 construct included an ampicillin resistance gene and was transformed into *E. coli* BL21(DE3) cells. An overnight culture of a single colony was diluted 1:100 into 2 L LB that was supplemented with 100 μ g/mL ampicillin. The culture was incubated with shaking at 37°C and when an OD_{600nm} of 0.4 – 0.6 was reached, protein expression was induced with the addition of IPTG to a final concentration of 1 mM. The culture was further incubated at 25°C for 16 h with agitation. The cells were then harvested by centrifugation (15 min, 14,000g), resuspended in equilibration buffer (50 mM Tris-HCl, pH 7.5, 150 mM NaCl, 10 mM imidazole), and subjected to sonication on ice. The lysate was cleared by centrifugation (50 min, 10,000g) and the supernatant was loaded onto HiTrap HP nickel affinity column 5 mL (GE Healthcare) pre-equilibrated with equilibration buffer. The column was then washed with equilibration buffer (20× column volume). The His_{6x}-MBP-Rv1155 fusion protein was released from the column with elution buffer (50 mM Tris-HCl, pH 7.5, 150 mM NaCl, 300 mM imidazole). The eluted protein was exchanged into a buffer optimized for the TEV protease cleavage reaction (50 mM Tris-HCl, pH 7.5, 150 mM NaCl, 0.5 mM EDTA, 1 mM DTT) using 10 kDa cutoff centrifugation filters (Millipore). The tag was efficiently cleaved by incubation with TEV protease (1:100 molar ratio) at 25°C for 2 h. The His_{6x}-TEV and any uncleaved His_{6x}-MBP-Rv1155 were removed from the reaction mixture by loading it onto a second HiTrap HP nickel affinity column with a 50 mL superloop (GE Healthcare). The cleaved Rv1155 without a His_{6x} tag also bound the nickel column, but was eluted with high salt buffer (50 mM Tris-HCl, pH 7.5, 600 mM NaCl, 10 mM imidazole), leaving the His_{6x}-tagged proteins on the nickel affinity resin. The Rv1155 that was eluted from the second HiTrap column was pooled and exchanged into equilibration buffer.

For protein to be used for crystallization experiments, F₄₂₀ was added to Rv1155 (4:1 molar ratio of coenzyme to enzyme) and incubated at 4°C overnight. The complex was then purified by SEC using a Superdex-75 10/300 GL column (GE Healthcare) pre-equilibrated with 10 mM Tris-HCl, pH 7.5, 50 mM NaCl, and 50 μ M F₄₂₀. The eluate was monitored at two wavelengths: $\lambda_1 = 280$ nm (protein) and $\lambda_2 = 420$ nm (F₄₂₀). The column fractions that absorbed at both 280 nm and 420 nm were analyzed by SDS-PAGE. Fractions containing pure Rv1155-F₄₂₀ were pooled and concentrated to 10 mg/mL with 10 kDa cutoff centrifugation filters (Millipore). For protein to be used for ITC experiments, the pooled cleaved Rv1155 eluted from the second HiTrap column was purified by SEC with a 16/60 Superdex-75 column (GE Healthcare) pre-

equilibrated with 50 mM potassium phosphate buffer, pH 7.5, 50 mM NaCl. Fractions containing pure Rv1155 were pooled and concentrated to 10 mg/mL with 10 kDa cutoff centrifugation filters (Millipore). The yield was 10 mg of Rv1155 per 1 L of cells. Rv1155 purified by SEC was a >95% pure homodimer as assessed by SDS-PAGE of column fractions. The mass of one untagged Rv1155 monomer was determined to be 16227.0 Da by mass spectrometry, which is the calculated molecular weight of Rv1155 without the initiating methionine and with an extra glycine residue remaining after TEV cleavage.

Differential scanning fluorimetry

Samples (100 μ L) contained 5 μ M Rv1155, 2.5 \times SYPRO[®] Orange (Invitrogen), 100 mM potassium phosphate buffer pH 7.8, 100 mM NaCl, and either 50 μ M cofactor (FMN, FAD, NADPH, or F₄₂₀) or an equivalent volume of water as a negative control.²⁰ Samples were placed in a MicroAmp[®] optical 96-well reaction plate and sealed with optical adhesive film (Applied Biosystems). All samples were tested in triplicate over a temperature range of 40–75°C with a ramp rate of 0.01°C/s, collecting a scan every 1 s. Fluorescence data were collected on a 7500 Real Time PCR instrument using the ROX[™] filter (λ_{ex} : 587 nm, λ_{em} : 607 nm). Data were analyzed using Protein Thermal Shift v1.0 software (Applied Biosystems). The T_m was determined by calculating the negative derivative of the melt curve and identifying the local minimum.

Isothermal titration calorimetry

Untagged Rv1155 (without added F₄₂₀) underwent dialysis overnight at 4°C with stirring in a 10 kDa MW cutoff Slide-A-Lyzer dialysis cassette (ThermoScientific, US) against 600 mL of 100 mM potassium phosphate buffer pH 7.4 and 20 mM NaCl. F₄₂₀ was dialyzed into the same buffer using a 500 Da cutoff Float-A-Lyzer dialysis cassette (Spectrum Laboratories, CA). The dialysate was retained to rinse the instrument before use. For the titration of F₄₂₀ into Rv1155, 879 μ M F₄₂₀ and 50 μ M Rv1155 were used.

All titrations were performed on a MicroCal VP-ITC calorimeter (GE Healthcare). In general, experimental parameters were as follows: thirty 10 μ L injections (5 μ L for first injection) with 20 s duration (10 s for the first injection), 5–7 μ cal/s reference power, 120 s initial delay, and 300 s spacing. The cell temperature was held at 30°C. The titration of F₄₂₀ into Rv1155 (50 μ M monomer) was conducted under low c value conditions, where $c = [M]_f/K_D$ and $[M]_t$ is the total protein concentration.⁴⁴ To achieve a higher c value in the ITC experiment, protein concentrations >50 μ M were attempted, but led to protein aggregation. Data were analyzed and figures

were generated using Origin software (OriginLab Corp).

Trial enzymatic reactions

All activity assays for Rv1155 were conducted using a Varian Cary 300 Bio UV-Visible spectrophotometer in 1 cm path length quartz cuvettes (Varian). Where present, the reagents were at the following concentrations: 1 μ M Rv1155, 100 μ M test substrate, 20 μ M F₄₂₀ or F₄₂₀H₂. Reaction mixtures (150 μ L total) contained: (1) Rv1155, substrate, and F₄₂₀ or F₄₂₀H₂, (2) Rv1155 and substrate, (3) substrate and F₄₂₀ or F₄₂₀H₂, (4) Rv1155 and F₄₂₀ or F₄₂₀H₂. Test substrates were pyridoxine 5'-phosphate, pyridoxamine 5'-phosphate, PLP, PA-824, coumarin, 7-hydroxycoumarin, 7-hydroxy-4-methylcoumarin, and imperatorin. All reactions were carried out in 25 mM potassium phosphate, pH 7.5. The reactions were initiated with the addition of enzyme and a wavelength scan (200–500 nm) was collected every 2 min for 1 h.

Rv1155–F₄₂₀ crystals, X-ray data, and structure determination

Crystallization trials were carried out using a Crystal Phoenix crystallization robot (Art Robbins Instruments LLC) to set up the binary complex Rv1155–F₄₂₀ with the conditions from the Classics, JCSG Core I–IV, pH Clear, and PEGs Suite crystallization kits (Qiagen). A number of buffer conditions produced crystals, including 0.1M MES, 25% PEG-3350 or PEG-4000 or PEG-6000 or PEG-8000 and 0.2M sodium or potassium fluoride, 20% PEG-3350, and 0.2M sodium or potassium formate, 20% PEG-3350. Crystals grown in 0.2M sodium fluoride, 20% PEG-3350 or in 0.2M sodium formate, 20% PEG-3350 exhibited the highest resolution diffraction.

Crystallization trials with Rv1155–F₄₂₀ yielded initial crystals of the Rv1155 dimer in which only one monomer contained a bound F₄₂₀ molecule. Optimization studies succeeded in filling the second binding site by soaking briefly in a cryoprotectant solution with additional F₄₂₀ (1 mM). All Rv1155–F₄₂₀ crystals, whether there were one or two molecules of F₄₂₀ bound, exhibited the same space group (P2₁2₁2₁) with unit cell dimensions of about 54, 65, and 77 Å. Rv1155 apoenzyme crystallized in the space group P2₁ and had unit cell dimensions of about 47, 55, 55 Å, $\beta = 108^\circ$, similar to other apoenzyme crystals.^{18,19} In the absence of F₄₂₀, the crystals grew as thin plates, but in the presence of F₄₂₀ the crystals appeared as tetragonal bipyramids. For X-ray data collection, Rv1155 crystals were briefly soaked in a cryoprotectant buffer consisting of 0.2M sodium formate, 20% PEG-3350, 25% glycerol, and 1 mM F₄₂₀, and then were rapidly frozen in liquid nitrogen. X-ray data were collected at –180°C at beamline 22 at the Advanced Photon Source

(Argonne National Laboratory, Lemont, IL). Initial phases were obtained by molecular replacement with an Rv1155 model (PDBID: 1Y30¹⁹) after removing ligands. Refinement of the structure with Crystallography and NMR System (CNS),⁴⁵ Phenix,⁴⁶ and model rebuilding with the O software⁴⁷ resulted in an R_{free} of 0.25 and an R_{work} of 0.19 at 2.3 Å resolution. Structural images were produced with Chimera.²³ The Rv1155–F₄₂₀ coordinates and structure factors were deposited into the Protein Data Bank (<http://www.rcsb.org>) as PDBID 4QVB.

Metabolic pathway analysis for Rv1155

We used the Search Tool for Retrieval of Interacting Genes/Proteins (STRING) v9.1⁴⁸ with Rv1155 as the seed protein to identify possible functional partners using the following prediction methods: gene fusion, co-occurrence, co-expression, experiments, databases, and text mining. A high confidence combined score of 0.7 was used as a cutoff. From the top 20 hits, those co-occurring with Rv1155 were selected for further analysis including signal peptide prediction with SignalP 4.1⁴⁹ (<http://www.cbs.dtu.dk/services/SignalP/>), transmembrane prediction using the TMHMM server v2.0⁵⁰ (<http://www.cbs.dtu.dk/services/TMHMM/>), amphipathic membrane anchors using AmphipaseK⁵¹ (http://npsa-pbil.ibcp.fr/cgi-bin/npsa_automat.pl?page=/NPSA/npsa_amphipaseek.html), and cell localization using the TubercuList database⁵² (<http://tuberculist.epfl.ch/index.html>).

Acknowledgments

The authors thank Dr. Tathagata Mukherjee (Genova Biopharmaceuticals) for his assistance in developing the protocol to purify coenzyme F₄₂₀. They also thank Dr. Marko Hyvönen (Department of Biochemistry, University of Cambridge) for useful discussions. EHM acknowledges the support of the NIH Oxford-Cambridge Scholars Program. X-ray data were collected at the Southeast Regional Collaborative Access Team (SER-CAT) 22-ID and 22-BM beam lines at the Advanced Photon Source (APS), which is supported by the U. S. Department of Energy, Office of Science, Office of Basic Energy Sciences under contract W-31-109-Eng-38.

References

1. Koul A, Arnoult E, Lounis N, Guillemont J, Andries K (2011) The challenge of new drug discovery for tuberculosis. *Nature* 469:483–490.
2. Raviglione M, Marais B, Floyd K, Lonroth K, Getahun H, Migliori GB, Harries AD, Nunn P, Lienhardt C, Graham S, Chakaya J, Weyer K, Cole S, Kaufmann SH, Zumla A (2012) Scaling up interventions to achieve global tuberculosis control: progress and new developments. *Lancet* 379:1902–1913.
3. Barry CE, III, Boshoff HI, Dowd CS (2004) Prospects for clinical introduction of nitroimidazole antibiotics for

the treatment of tuberculosis. *Curr Pharm Des* 10: 3239–3262.

4. Cheeseman P, Toms-Wood A, Wolfe RS (1972) Isolation and properties of a fluorescent compound, factor 420, from *Methanobacterium* strain M.o.H. *J Bacteriol* 112: 527–531.
5. Bair TB, Isabelle DW, Daniels L (2001) Structures of coenzyme F₄₂₀ in *Mycobacterium* species. *Arch Microbiol* 176:37–43.
6. Stover CK, Warrener P, VanDevanter DR, Sherman DR, Arain TM, Langhorne MH, Anderson SW, Towell JA, Yuan Y, McMurray DN, Kreiswirth BN, Barry CE, III, Baker WR (2000) A small-molecule nitroimidazopyran drug candidate for the treatment of tuberculosis. *Nature* 405:962–966.
7. Ginsberg AM, Laurenzi MW, Rouse DJ, Whitney KD, Spigelman MK (2009) Safety, tolerability, and pharmacokinetics of PA-824 in healthy subjects. *Antimicrob Agents Chemother* 53:3720–3725.
8. Cousins FB (1960) The prosthetic group of a chromoprotein from mycobacteria. *Biochim Biophys Acta* 40: 532–534.
9. Sutton WB (1964) Properties of a new TPN-like electron transport component from *Mycobacterium phlei*. *Biochem Biophys Res Commun* 15:414–419.
10. Walsh C (1986) Naturally occurring 5-deazaflavin coenzymes: biological redox roles. *Acc Chem Res* 19:216–221.
11. Bugg TDH (2004) Introduction to enzyme and coenzyme chemistry. Oxford: Blackwell Publishing Ltd.
12. Boshoff HI, Barry CE, III (2005) Tuberculosis—metabolism and respiration in the absence of growth. *Nat Rev Microbiol* 3:70–80.
13. Selengut JD, Haft DH (2010) Unexpected abundance of coenzyme F₄₂₀-dependent enzymes in *Mycobacterium tuberculosis* and other actinobacteria. *J Bacteriol* 192: 5788–5798.
14. Manjunatha UH, Boshoff H, Dowd CS, Zhang L, Albert TJ, Norton JE, Daniels L, Dick T, Pang SS, Barry CE (2006) Identification of a nitroimidazo-oxazine-specific protein involved in PA-824 resistance in *Mycobacterium tuberculosis*. *Proc Natl Acad Sci USA* 103:431–436.
15. Bashiri G, Squire CJ, Moreland NJ, Baker EN (2008) Crystal structures of F₄₂₀-dependent glucose-6-phosphate dehydrogenase FGD1 involved in the activation of the anti-tuberculosis drug candidate PA-824 reveal the basis of coenzyme and substrate binding. *J Biol Chem* 283:17531–17541.
16. Purwantini E, Daniels L (1996) Purification of a novel coenzyme F₄₂₀-dependent glucose-6-phosphate dehydrogenase from *Mycobacterium smegmatis*. *J Bacteriol* 178:2861–2866.
17. Mashalidis EH, Mukherjee T, Sledz P, Matak-Vinkovic D, Boshoff H, Abell C, Barry CE, III (2011) Rv2607 from *Mycobacterium tuberculosis* is a pyridoxine 5'-phosphate oxidase with unusual substrate specificity. *PLoS One* 6:e27643.
18. Canaan S, Sulzenbacher G, Roig-Zamboni V, Scappuccini-Calvo L, Frassinetti F, Maurin D, Cambillau C, Bourne Y (2005) Crystal structure of the conserved hypothetical protein Rv1155 from *Mycobacterium tuberculosis*. *FEBS Lett* 579:215–221.
19. Biswal BK, Cherney MM, Wang M, Garen C, James MN (2005) Structures of *Mycobacterium tuberculosis* pyridoxine 5'-phosphate oxidase and its complexes with flavin mononucleotide and pyridoxal 5'-phosphate. *Acta Crystallogr D Biol Crystallogr* 61:1492–1499.
20. Mashalidis EH, Sledz P, Lang S, Abell C (2013) A three-stage biophysical screening cascade for fragment-based drug discovery. *Nat Protoc* 8:2309–2324.

21. Cellitti SE, Shaffer J, Jones DH, Mukherjee T, Gurumurthy M, Bursulaya B, Boshoff HI, Choi I, Nayyar A, Lee YS, Cherian J, Niyomrattanakit P, Dick T, Manjunatha UH, Barry CE, III, Spraggon G, Geierstanger BH (2012) Structure of Ddn, the deazaflavin-dependent nitroreductase from *Mycobacterium tuberculosis* involved in bioreductive activation of PA-824. *Structure* 20:101–112.
22. Taylor MC, Jackson CJ, Tattersall DB, French N, Peat TS, Newman J, Briggs LJ, Lalalikar GV, Campbell PM, Scott C, Russell RJ, Oakeshott JG (2010) Identification and characterization of two families of F₄₂₀H₂-dependent reductases from *Mycobacteria* that catalyse aflatoxin degradation. *Mol Microbiol* 78:561–575.
23. Pettersen EF, Goddard TD, Huang CC, Couch GS, Greenblatt DM, Meng EC, Ferrin TE (2004) UCSF Chimera—a visualization system for exploratory research and analysis. *J Comput Chem* 25:1605–1612.
24. Moonen CT, Vervoort J, Muller F (1984) Carbon-13 nuclear magnetic resonance study on the dynamics of the conformation of reduced flavin. *Biochemistry* 23:4868–4872.
25. Walsh JD, Miller A-F (2003) Flavin reduction potential tuning by substitution and bending. *J Mol Struct: Theochem* 623:185–195.
26. Dundas J, Ouyang Z, Tseng J, Binkowski A, Turpaz Y, Liang J (2006) CASTp: computed atlas of surface topography of proteins with structural and topographical mapping of functionally annotated residues. *Nucleic Acids Res* 34:W116–W118.
27. Safo MK, Musayev FN, di Salvo ML, Schirch V (2001) X-ray structure of *Escherichia coli* pyridoxine 5'-phosphate oxidase complexed with pyridoxal 5'-phosphate at 2.0 Å resolution. *J Mol Biol* 310:817–826.
28. Musayev FN, Di Salvo ML, Ko TP, Schirch V, Safo MK (2003) Structure and properties of recombinant human pyridoxine 5'-phosphate oxidase. *Protein Sci* 12:1455–1463.
29. Holm L, Rosenstrom P (2010) Dali server: conservation mapping in 3D. *Nucleic Acids Res* 38:W545–W549.
30. Biswal BK, Au K, Cherney MM, Garen C, James MN (2006) The molecular structure of Rv2074, a probable pyridoxine 5'-phosphate oxidase from *Mycobacterium tuberculosis*, at 1.6 Å resolution. *Acta Crystallogr Sect F Struct Biol Cryst Commun* 62:735–742.
31. Malen H, Pathak S, Softeland T, de Souza GA, Wiker HG (2010) Definition of novel cell envelope associated proteins in Triton X-114 extracts of *Mycobacterium tuberculosis* H37Rv. *BMC Microbiol* 10:132–142.
32. von Mering C, Huynen M, Jaeggi D, Schmidt S, Bork P, Snel B (2003) STRING: a database of predicted functional associations between proteins. *Nucleic Acids Res* 31:258–261.
33. Pellegrini M, Marcotte EM, Thompson MJ, Eisenberg D, Yeates TO (1999) Assigning protein functions by comparative genome analysis: protein phylogenetic profiles. *Proc Natl Acad Sci USA* 96:4285–4288.
34. Bateman A, Coin L, Durbin R, Finn RD, Hollich V, Griffiths-Jones S, Khanna A, Marshall M, Moxon S, Sonnhammer EL, Studholme DJ, Yeats C, Eddy SR (2004) The Pfam protein families database. *Nucleic Acids Res* 32:D138–D141.
35. Warkentin E, Mamat B, Sordel-Klippert M, Wicke M, Thauer RK, Iwata M, Iwata S, Ermler U, Shima S (2001) Structures of F₄₂₀H₂:NADP⁺ oxidoreductase with and without its substrates bound. *EMBO J* 20:6561–6569.
36. Ceh K, Demmer U, Warkentin E, Moll J, Thauer RK, Shima S, Ermler U (2009) Structural basis of the hydride transfer mechanism in F₄₂₀-dependent methylenetetrahydromethanopterin dehydrogenase. *Biochemistry* 48:10098–10105.
37. Aufhammer SW, Warkentin E, Berk H, Shima S, Thauer RK, Ermler U (2004) Coenzyme binding in F₄₂₀-dependent secondary alcohol dehydrogenase, a member of the bacterial luciferase family. *Structure* 12:361–370.
38. Aufhammer SW, Warkentin E, Ermler U, Hagemeyer CH, Thauer RK, Shima S (2005) Crystal structure of methylenetetrahydromethanopterin reductase (Mer) in complex with coenzyme F₄₂₀: architecture of the F₄₂₀/FMN binding site of enzymes within the nonprolyl cis-peptide containing bacterial luciferase family. *Protein Sci* 14:1840–1849.
39. Bashiri G, Rehan AM, Greenwood DR, Dickson JM, Baker EN (2010) Metabolic engineering of cofactor F₄₂₀ production in *Mycobacterium smegmatis*. *PLoS One* 5:e15803.
40. Isabelle D, Simpson DR, Daniels L (2002) Large-scale production of coenzyme F₄₂₀-5,6 by using *Mycobacterium smegmatis*. *Appl Environ Microbiol* 68:5750–5755.
41. Choi KP, Kendrick N, Daniels L (2002) Demonstration that *fbtC* is required by *Mycobacterium bovis* BCG for coenzyme F₄₂₀ and FO biosynthesis. *J Bacteriol* 184:2420–2428.
42. Bashiri G, Squire CJ, Baker EN, Moreland NJ (2007) Expression, purification and crystallization of native and selenomethionine labeled *Mycobacterium tuberculosis* FGD1 (Rv0407) using a *Mycobacterium smegmatis* expression system. *Protein Expr Purif* 54:38–44.
43. Ashby KD, Casey TA, Rasmussen MA, Petrich JW (2001) Steady-state and time-resolved spectroscopy of F₄₂₀ extracted from methanogen cells and its utility as a marker for fecal contamination. *J Agric Food Chem* 49:1123–1127.
44. Turnbull WB, Precious BL, Homans SW (2004) Dissecting the cholera toxin-ganglioside GM1 interaction by isothermal titration calorimetry. *J Am Chem Soc* 126:1047–1054.
45. Brunger AT (2007) Version 1.2 of the crystallography and NMR system. *Nat Protoc* 2:2728–2733.
46. Adams PD, Afonine PV, Bunkoczi G, Chen VB, Davis IW, Echols N, Headd JJ, Hung LW, Kapral GJ, Grosse-Kunstleve RW, McCoy AJ, Moriarty NW, Oeffner R, Read RJ, Richardson DC, Richardson JS, Terwilliger TC, Zwart PH (2010) PHENIX: a comprehensive Python-based system for macromolecular structure solution. *Acta Crystallogr D Biol Crystallogr* 66:213–221.
47. Jones TA (2004) Interactive electron-density map interpretation: from INTER to O. *Acta Crystallogr D Biol Crystallogr* 60:2115–2125.
48. Franceschini A, Szklarczyk D, Frankild S, Kuhn M, Simonovic M, Roth A, Lin J, Minguez P, Bork P, von Mering C, Jensen LJ (2013) STRING v9.1: protein-protein interaction networks, with increased coverage and integration. *Nucleic Acids Res* 41:D808–D815.
49. Petersen TN, Brunak S, von Heijne G, Nielsen H (2011) SignalP 4.0: discriminating signal peptides from transmembrane regions. *Nat Methods* 8:785–786.
50. Krogh A, Larsson B, von Heijne G, Sonnhammer EL (2001) Predicting transmembrane protein topology with a hidden Markov model: application to complete genomes. *J Mol Biol* 305:567–580.
51. Sapay N, Guermeur Y, Deleage G (2006) Prediction of amphipathic in-plane membrane anchors in monotopic proteins using a SVM classifier. *BMC Bioinformatics* 7:255.
52. Lew JM, Kapopoulou A, Jones LM, Cole ST (2011) TubercuList—10 years after. *Tuberculosis (Edinb)* 91:1–7.